Electronic Supplementary Material (ESI) for Faraday Discussions.

Intermediate-spin iron(IV)-oxido species with record reactivity

Supporting Information

Peter Comba[a,b], George Nunn[c], Frederik Scherz[a], Paul H. Walton[c]*

a) Universität Heidelberg, Anorganisch-Chemisches Institut, INF 270,

D-69120 Heidelberg, Germany

b) Universität Heidelberg, Interdisziplinäres Zentrum für Wissenschaftliches Rechnen (IWR)

c) Department of Chemistry, University of York, Heslington, York, YO10 5DD, UK

Supporting Information

Correspondence:
E-mail: peter.comba@aci.uni-heidelberg.de

Table of Contents

Table of Contents 2
Ligand Field Analysis 3
Ligand field analysis of $[(L^2)Fe^{IV}=O(MeCN)]^{2+}$ 3
Ligand field analysis of $[(L^1)Fe^{IV}=O(X)]^{n+}$ (X = MeCN, Cl^-, Br^-) 4
Orbital diagrams 6
Calculated transitions 10
Calculated zero-field splitting parameters 23
References 23

Ligand Field Analysis

Ligand field analysis of $[(L^2)Fe^{IV}=O(MeCN)]^{2+}$

The electronic structure of $[(L^2)Fe^{IV}=O(MeCN)]^{2+}$ has C_{4v} symmetry with five allowed one-electron transitions. The ground state electronic configuration $(d_{xy})^2(d_{xz})^1(d_{yz})^1(d_{x^2-y^2})(d_{z^2})$ is achieved by setting $2e_\sigma$(axial) > $3e_\sigma$(equatorial) > e_π(axial). Five experimental d-d transitions[1] have been assigned to spin-allowed transitions at 10400 cm^{-1} ($d_{xy} \rightarrow d_{x^2-y^2}$), 10600 cm^{-1} ($d_{xy} \rightarrow d_{xz/yz}$), 12900 cm^{-1} ($d_{xz/yz} \rightarrow d_{x^2-y^2}$), 17600 cm^{-1} ($d_{xz/yz} \rightarrow d_{z^2}$) and 25000 cm^{-1} ($d_{xy} \rightarrow d_{z^2}$). The three e_λ parameters were varied along with Racah B and a C/B. An idealised octahedral geometry is used.

Despite repeated attempts, it was not possible to assign the low energy band at 10400 cm^{-1} to the spin allowed $d_{xy} \rightarrow d_{x^2-y^2}$ whilst having the $d_{xz/yz} \rightarrow d_{x^2-y^2}$ transition higher in energy; most attempts to do so assigned the molecule a quintet ground state ($^5B_1$) and placed the $d_{xz/yz} \rightarrow d_{x^2-y^2}$ transition at around 6000 cm^{-1}. This is not a possibility given that the three transitions to and from d_{xz}/d_{yz} have been assigned as xy-polarised in the spectrum already and are accounted for by Kestrel. Instead a search of an alternative assignment was made.

There are only two other one-electron transitions that are z-polarised and they are the spin forbidden triplet to quintet transitions: $d_{xy} \rightarrow d_{x^2-y^2}$, $d_{xy} \rightarrow d_{z^2}$. Positioning one of these quintet bands at 10400 cm^{-1} allows for that transition to couple with the spin allowed transition at 10600 cm^{-1}. Calculations suggest that the energy separation between the triplet ground state and the quintet state are about 13 kcal/mol (~4500 cm^{-1}) which would be the $d_{xy} \rightarrow d_{x^2-y^2}$ transition meaning that the second quintet excited state (the $d_{xy} \rightarrow d_{z^2}$ transition) is the most likely assignment at 10400 cm^{-1}. The quintet excited state at 4500 cm^{-1} was fitted with a lower weight (0.1).

Fitting these new assignments by varying the e parameters and Racah B (C/B=5.0) afforded a good reproduction of the experimental spectrum. The spin forbidden band's appearence in the spectrum can be explained by the mixing of the triplet and quintet transitions under the effects of spin-orbit coupling (Table S1). If the quintet band is placed at ~10400 cm^{-1} and the low energy triplet transition at ~10600 cm^{-1} then recreation of the experimental zero-field splitting gives the spin orbit coupled split quintet states 31–47 % spin triplet character.

Table S1. Calculated SOC transitions of $[(L^2)Fe^{IV}=O(MeCN)]^{2+}$

				Spin Projections		
States	**Deg**	**Mult**	**dE (cm-1)**	**5**	**3**	**1**
11–11	1	3	9929.3	0.43	0.56	0.01
12–12	1	3	9952.9	0.45	0.55	0
13–14	2	5	10193.6	**0.53**	**0.47**	0
15–15	1	5	10339.9	**0.69**	**0.31**	0
16–16	1	3	10747.8	0	0.99	0.01
17–18	2	3	10867.5	0.46	0.54	0
19–19	1	3	10913	0.3	0.69	0
20–20	1	5	10916.1	**0.55**	**0.44**	0.01
21–21	1	5	10933.3	**0.53**	**0.47**	0

This assignment also places the triplet double electron jump $d_{xy} \rightarrow d_{x^2-y^2}$ transitions in the 20000 cm^{-1} to 23300 cm^{-1} (average 21080 cm^{-1}) which coincides with an unidentified peak in the experimental MCD spectra which has negligible intensity in the UV-vis. The triplet $d_{xy} \rightarrow d_{x^2-y^2}$ transition lies close to the $d_{xz/yz} \rightarrow d_{z^2}$ transition. Further to this, using the DFT optimised geometry does not perturb the calculated energies to any significant extent.

The assignment of the spin forbidden band allows a reasonable estimation of Racah B and C. This assignment, which is thought to be reported here as a possibility first, requires further analysis that is beyond the scope of this work.

Ligand field analysis of $[(L^1)Fe^{IV}=O(X)]^{n+}$ (X = MeCN, Cl^-, Br^-)

The UV-Vis spectra were analysed via a gaussian deconvolution to find the position of the bands, the results of which are given in Table S2. The spectra featured a low-resolution shoulder at around 900 nm and was included in the deconvolution. It should be noted that the spectra were carried out at –90 °C and not of a high resolution.

Table S2. Gaussian analysis of the UV-vis spectra of $[(L^1)Fe^{IV}=O(X)]^{n+}$ (X = MeCN, Cl^-, Br^-)

X	LF bands / cm^{-1} (nm)
MeCN	19011 (526), 13004 (769), 10432 (959)
Cl^-	17211 (581), 12034 (831), 10331 (968)
Br^-	16474 (607), 11933 (838), 10737 (931)

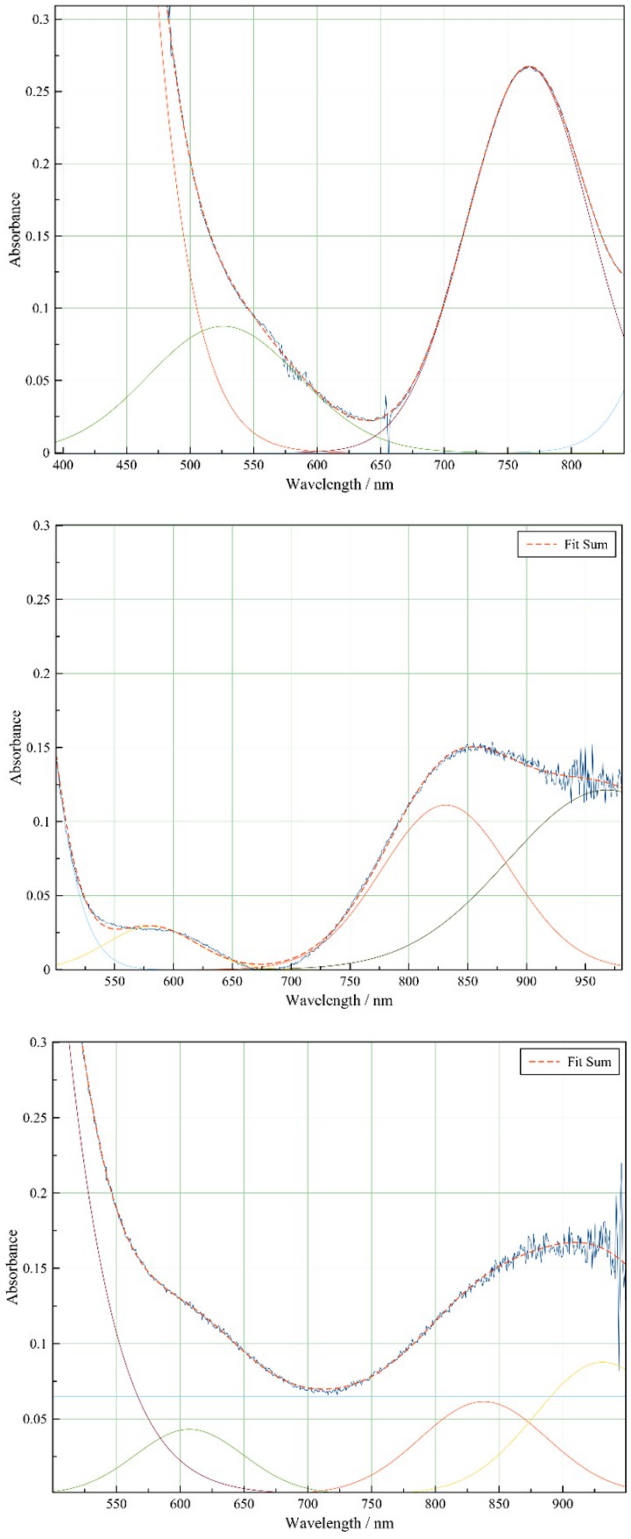

Figure S1. Gaussian deconvolution of the UV-vis spectra of $[(L^1)Fe^{IV}=O(X)]^{n+}$ (from top to bottom: X = MeCN, Cl^-, Br^-; note that the resolution of the experimental spectra (cryo-stopped-flow) is limited; in the main text we have adopted the values determined here except fot the Br^- complex, where the low energy transition was set to 900 nm).

The axial AOM parameters from $[(L^2)Fe^{IV}=O(MeCN)]^{2+}$ were transferred to the octahedral geometry and were fixed. The Racah C/B ratio was fixed at 5.0. The equatorial e_σ values were varied along with the Racah B parameter.

A value of Racah B at ~600 cm^{-1} was enough to correlate the band gap with the e_σ(equatorial) parameter. It was found that the average e_σ decreased going from MeCN > Cl^- > Br^-. The shoulders were positioned approximately within range of the deconvoluted band (although there is a larger error on this).

Orbital diagrams

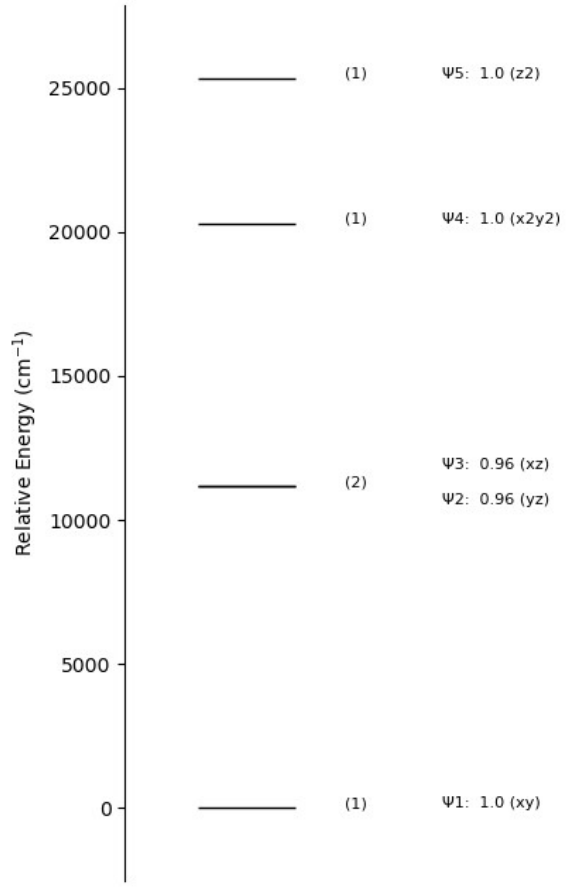

Scheme S1. L^2 / MeCN computed orbital energies.

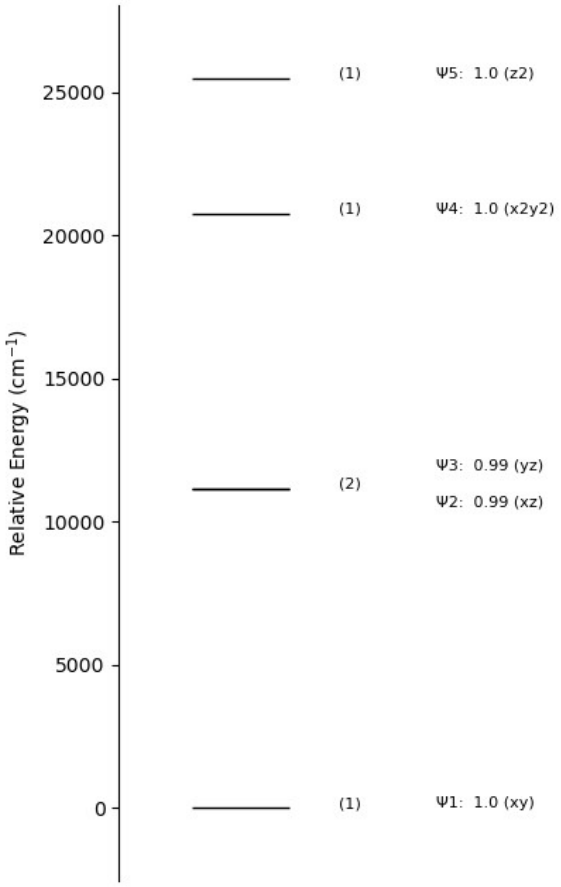

Scheme S2. L^1 / MeCN computed orbital energies.

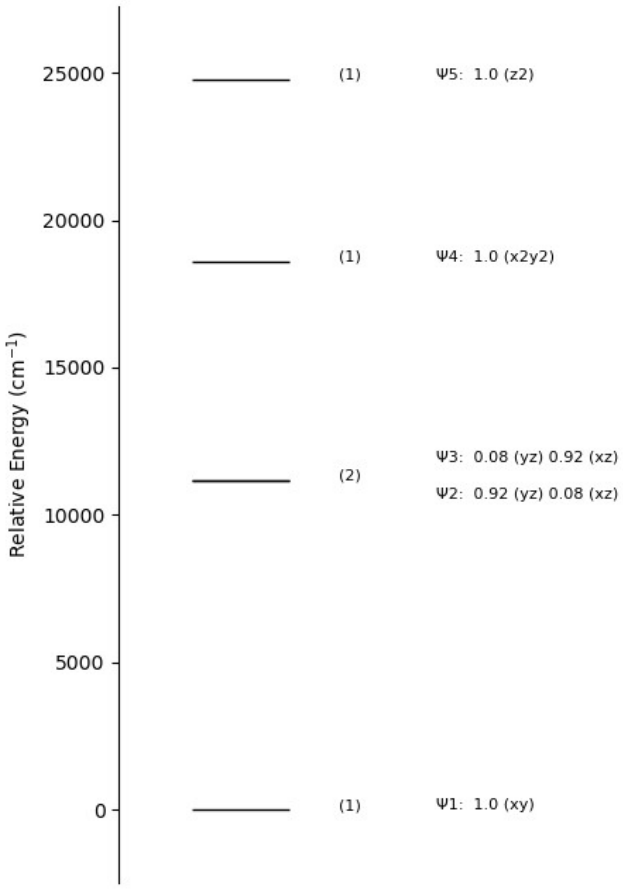

Scheme S3. L^1 / Cl^- computed orbital energies.

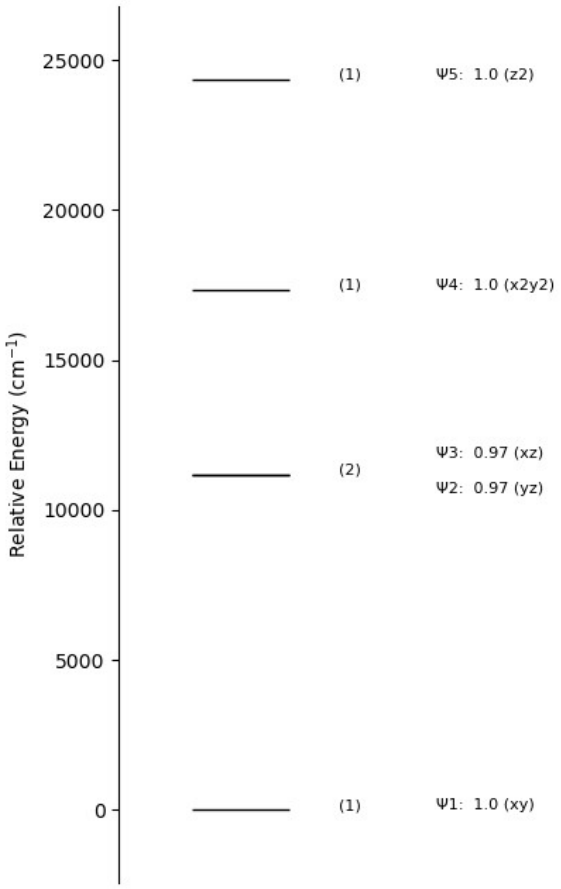

Scheme S4. L^1 / Br^- computed orbital energies.

Calculated transitions

All spectra were calculated with a development version of the LFT program Kestrel.

Data includes all transitions up to 30000 cm^{-1}.

Without SOC

Table S3. L^2 / MeCN computed transitions, Racah B = 500, C/B = 5, no SOC.

				Spin Projections		
States	**Deg**	**Mult**	**dE (cm-1)**	**5**	**3**	**1**
1–3	3	3	0	0	1	0
4–8	5	5	5436	1	0	0
9–9	1	1	7107.3	0	0	1
10–10	1	1	7674.2	0	0	1
11–15	5	5	10472.2	1	0	0
16–21	6	3	10488	0	1	0
22–22	1	1	12214.8	0	0	1
23–28	6	3	12812.2	0	1	0
29–30	2	1	16447.4	0	0	1
31–36	6	3	17567.8	0	1	0
37–39	3	3	18287.1	0	1	0
40–49	10	5	19613.4	1	0	0
50–52	3	3	19953.5	0	1	0
53–54	2	1	20219.3	0	0	1
55–57	3	3	20315.6	0	1	0
58–60	3	3	21081.8	0	1	0
61–63	3	3	22471.4	0	1	0
64–66	3	3	22667.4	0	1	0
67–67	1	1	25110.7	0	0	1
68–68	1	1	25147.5	0	0	1
69–70	2	1	25224.5	0	0	1
71–73	3	3	25263.6	0	1	0
74–74	1	1	25681.9	0	0	1
75–77	3	3	25771.8	0	1	0
78–78	1	1	29258.4	0	0	1

79–81	3	3	29444.6	0	1	0
82–82	1	1	29711.4	0	0	1
83–85	3	3	30153.2	0	1	0

Table S4. L^1 / MeCN, computed transitions.

				Spin Projections		
States	**Deg**	**Mult**	**dE (cm-1)**	**5**	**3**	**1**
1–3	3	3	0	0	1	0
4–8	5	5	2653.6	1	0	0
9–13	5	5	7377.6	1	0	0
14–14	1	1	8584.4	0	0	1
15–15	1	1	9320.2	0	0	1
16–21	6	3	10388.4	0	1	0
22–27	6	3	13050	0	1	0
28–28	1	1	14352.4	0	0	1
29–38	10	5	16987.1	1	0	0
39–40	2	1	17835	0	0	1
41–43	3	3	18373.6	0	1	0
44–49	6	3	19049.9	0	1	0
50–52	3	3	20279.7	0	1	0
53–55	3	3	20574.3	0	1	0
56–57	2	1	21657.2	0	0	1
58–60	3	3	21724.1	0	1	0
61–63	3	3	22514.5	0	1	0
64–66	3	3	22744.5	0	1	0
67–69	3	3	25764.7	0	1	0
70–72	3	3	26246.3	0	1	0
73–73	1	1	26607.6	0	0	1
74–74	1	1	26687.1	0	0	1
75–75	1	1	27300.4	0	0	1
76–80	5	5	28155.3	1	0	0
81–82	2	1	28653.3	0	0	1

83–85	3	3	30813.2	0	1	0
86–86	1	1	31019.5	0	0	1
87–87	1	1	31341.5	0	0	1
88–93	6	3	31419.4	0	1	0

Table S5. L^1 / Cl, computed transitions.

				Spin Projections		
States	**Deg**	**Mult**	**dE (cm-1)**	**5**	**3**	**1**
1–3	3	3	0.0	0	1	0
4–8	5	5	3205.3	1	0	0
9–9	1	1	4941.1	0	0	1
10–10	1	1	5338.9	0	0	1
11–16	6	3	7868.6	0	1	0
17–17	1	1	8736.3	0	0	1
18–23	6	3	9934.5	0	1	0
24–25	2	1	11556.4	0	0	1
26–28	3	3	11948.6	0	1	0
29–31	3	3	13666.7	0	1	0
32–34	3	3	13862.2	0	1	0
35–37	3	3	14289.4	0	1	0
38–42	5	5	15205.3	1	0	0
43–48	6	3	16681.9	0	1	0
49–49	1	1	16755.9	0	0	1
50–50	1	1	16911.2	0	0	1
51–52	2	1	17173.8	0	0	1
53–53	1	1	17253.3	0	0	1
54–56	3	3	17676.3	0	1	0
57–66	10	5	19205.3	1	0	0
67–68	2	1	20138.5	0	0	1
69–71	3	3	21125.8	0	1	0
72–72	1	1	21263.1	0	0	1

73–78	6	3	21561.2	0	1	0
79–84	6	3	23909.4	0	1	0
85–86	2	1	24574.0	0	0	1
87–89	3	3	24650.9	0	1	0
90–92	3	3	25608.8	0	1	0
93–95	3	3	26110.0	0	1	0
96–96	1	1	26528.3	0	0	1
97–97	1	1	26662.7	0	0	1
98–100	3	3	27174.7	0	1	0
101–101	1	1	27338.6	0	0	1
102–104	3	3	27701.8	0	1	0
105–109	5	5	28405.3	1	0	0
110–115	6	3	28474.8	0	1	0
116–121	6	3	28799.6	0	1	0
122–124	3	3	29472.3	0	1	0

Table S6. L^1 / Br, computed transitions, Racah B = 400, C/B = 4, no SOC.

				Spin Projections		
States	**Deg**	**Mult**	**dE (cm-1)**	**5**	**3**	**1**
1–3	3	3	0	0	1	0
4–8	5	5	1.2	1	0	0
9–13	5	5	7013	1	0	0
14–14	1	1	8207.5	0	0	1
15–15	1	1	8882.3	0	0	1
16–21	6	3	9774.9	0	1	0
22–27	6	3	11497	0	1	0
28–37	10	5	13190.8	1	0	0
38–38	1	1	13661.8	0	0	1
39–41	3	3	15122.6	0	1	0
42–47	6	3	16289.3	0	1	0
48–49	2	1	16655.7	0	0	1

50–52	3	3	17151.7	0	1	0
53–55	3	3	17533.7	0	1	0
56–58	3	3	18446.2	0	1	0
59–61	3	3	20084.4	0	1	0
62–63	2	1	20271.9	0	0	1
64–66	3	3	20600.8	0	1	0
67–67	1	1	23221.6	0	0	1
68–68	1	1	23387.5	0	0	1
69–71	3	3	23799.9	0	1	0
72–72	1	1	23858.8	0	0	1
73–77	5	5	24359	1	0	0
78–80	3	3	24876.4	0	1	0
81–82	2	1	25235	0	0	1
83–88	6	3	27170.1	0	1	0
89–91	3	3	28154	0	1	0
92–92	1	1	28176.3	0	0	1
93–98	6	3	28302.1	0	1	0

with SOC

Table S7. L^2 / MeCN, computed transitions, ζ = 415.

				Spin Projections		
States	**Deg**	**Mult**	**dE (cm-1)**	**5**	**3**	**1**
1–1	1	3	0	0.01	0.99	0
2–3	2	3	28.1	0.01	0.99	0
4–5	2	5	5493.9	1	0	0
6–7	2	5	5522.6	0.99	0.01	0
8–8	1	5	5532	0.99	0.01	0
9–9	1	1	7105.4	0	0.02	0.98
10–10	1	1	7709.2	0	0.01	0.99
11–11	1	3	9929.3	0.43	0.56	0.01
12–12	1	3	9952.9	0.45	0.55	0
13–14	2	5	10193.6	0.53	0.47	0

15–15	1	5	10339.9	0.69	0.31	0
16–16	1	3	10747.8	0	0.99	0.01
17–18	2	3	10867.5	0.46	0.54	0
19–19	1	3	10913	0.3	0.69	0
20–20	1	5	10916.1	0.55	0.44	0.01
21–21	1	5	10933.3	0.53	0.47	0
22–22	1	1	12236.2	0	0.13	0.87
23–23	1	3	12827.8	0.02	0.98	0
24–25	2	3	12887.9	0.01	0.99	0
26–26	1	3	12901.8	0.02	0.87	0.11
27–27	1	3	12967.7	0.01	0.99	0
28–28	1	3	12976.6	0	0.99	0.01
29–30	2	1	16441.3	0	0.03	0.97
31–31	1	3	17569.3	0	1	0
32–32	1	3	17616.2	0	0.99	0
33–34	2	3	17624.6	0	0.98	0.02
35–35	1	3	17665.4	0	1	0
36–36	1	3	17692.9	0	1	0
37–38	2	3	18391	0	0.99	0.01
39–39	1	3	18398.5	0	1	0
40–41	2	5	19421.8	0.98	0.02	0
42–42	1	5	19571.4	0.98	0.02	0
43–43	1	5	19575.5	0.98	0.02	0
44–45	2	5	19659.5	0.82	0.18	0
46–46	1	5	19680.1	0.73	0.27	0
47–48	2	5	19718.1	0.84	0.16	0
49–49	1	5	19746.9	0.94	0.06	0
50–51	2	3	20119	0.08	0.5	0.41
52–52	1	3	20197.1	0.27	0.73	0
53–54	2	3	20264.2	0.19	0.51	0.29
55–55	1	3	20408.3	0.05	0.95	0
56–57	2	3	20520	0.04	0.69	0.26
58–59	2	3	21163.3	0.01	0.97	0.02

60–60	1	3	21180.8	0.01	0.99	0
61–61	1	3	22601.1	0.01	0.98	0
62–63	2	3	22635.6	0.02	0.98	0
64–64	1	3	22784.7	0.01	0.99	0
65–66	2	3	22818.1	0.01	0.97	0.01
67–68	2	1	25071.3	0	0.44	0.56
69–69	1	1	25140.1	0	0.25	0.75
70–70	1	1	25160.7	0	0.01	0.99
71–71	1	3	25407.4	0	0.75	0.25
72–73	2	3	25516.4	0	0.64	0.35
74–74	1	1	25734	0	0.01	0.99
75–75	1	3	25849.7	0	1	0
76–77	2	3	25898.5	0	0.92	0.08
78–78	1	1	29227.9	0.01	0.07	0.92
79–79	1	3	29485.9	0.03	0.97	0
80–81	2	3	29497.5	0.02	0.98	0
82–82	1	1	29742.5	0	0.02	0.98
83–83	1	3	30152.2	0.15	0.84	0.01
84–85	2	3	30229.4	0.02	0.98	0
86–86	1	3	30362.2	0.38	0.59	0.03
87–87	1	5	30368.7	0.57	0.38	0.05
88–89	2	5	30591.2	0.57	0.43	0

Table S8. L^1 / MeCN, computed transitions, ζ = 415.

				Spin Projections		
States	**Deg**	**Mult**	**dE (cm-1)**	**5**	**3**	**1**
1–1	1	3	0	0.03	0.97	0
2–3	2	3	36.5	0.02	0.98	0
4–5	2	5	2755.8	1	0	0
6–7	2	5	2813.4	0.98	0.02	0
8–8	1	5	2831.7	0.97	0.03	0
9–10	2	5	7379.5	0.97	0.03	0

11–12	2	5	7433.2	0.99	0.01	0
13–13	1	5	7450.8	0.99	0.01	0
14–14	1	1	8582.9	0	0.04	0.96
15–15	1	1	9366.2	0	0.03	0.97
16–16	1	3	10396.3	0.03	0.97	0
17–17	1	3	10420.9	0.03	0.97	0
18–19	2	3	10528.3	0.01	0.99	0
20–20	1	3	10708.6	0	0.97	0.03
21–21	1	3	10715.5	0.01	0.97	0.03
22–22	1	3	13001.9	0.01	0.97	0.02
23–23	1	3	13036	0.01	0.99	0
24–25	2	3	13136.3	0.01	0.99	0
26–26	1	3	13267.1	0.01	0.99	0.01
27–27	1	3	13288.8	0.01	0.98	0.01
28–28	1	1	14498.9	0	0.03	0.97
29–30	2	5	16867.6	0.99	0.01	0
31–32	2	5	17016.6	0.99	0.01	0
33–34	2	5	17130.5	0.98	0.01	0
35–35	1	5	17205.1	0.99	0.01	0
36–36	1	5	17225.4	0.99	0.01	0
37–38	2	5	17264.4	0.98	0.01	0.01
39–40	2	1	17813.9	0.01	0.11	0.88
41–41	1	3	18418.1	0	1	0
42–43	2	3	18517.3	0	0.92	0.08
44–44	1	3	19142.4	0	1	0
45–45	1	3	19176.7	0	1	0
46–48	3	3	19181.9	0	0.99	0.01
49–49	1	3	19200.9	0	1	0
50–51	2	3	20451.1	0.01	0.99	0.01
52–52	1	3	20454	0.01	0.99	0
53–54	2	3	20657.1	0	0.97	0.03
55–55	1	3	20679.8	0	1	0
56–57	2	1	21680.9	0	0.44	0.56

58–58	1	3	21844.1	0	1	0
59–60	2	3	21901.3	0	0.62	0.38
61–61	1	3	22667	0	0.99	0
62–63	2	3	22707.8	0	0.99	0.01
64–64	1	3	22880.8	0.01	0.99	0
65–66	2	3	22939.7	0.01	0.96	0.04
67–68	2	3	25854.8	0	0.99	0.01
69–69	1	3	25857.8	0	0.98	0.02
70–71	2	3	26356.6	0	0.99	0
72–72	1	3	26360.7	0	1	0
73–73	1	1	26678.5	0	0.02	0.98
74–74	1	1	26793.1	0	0.03	0.97
75–75	1	1	27385.8	0	0.01	0.99
76–76	1	5	28164.5	0.96	0.03	0
77–77	1	5	28168.8	0.97	0.03	0
78–79	2	5	28243.4	0.97	0.03	0
80–80	1	5	28270.4	0.97	0.03	0
81–82	2	1	28768.6	0	0.02	0.98
83–83	1	1	30910.3	0.01	0.22	0.77
84–86	3	3	30943.5	0.01	0.99	0
87–87	1	1	31366.1	0	0.04	0.96
88–88	1	3	31532.3	0.03	0.95	0.02
89–90	2	3	31564.8	0.01	0.98	0
91–91	1	3	31595.7	0	1	0
92–92	1	3	31646.7	0.01	0.99	0
93–93	1	3	31774.5	0.02	0.8	0.18
94–94	1	3	31967.7	0	0.97	0.03
95–96	2	3	31987.5	0	0.99	0.01
97–97	1	3	32735.2	0	0.99	0.01

Table S9. L^1 / Cl, computed transitions, ζ = 415.

				Spin Projections		
States	**Deg**	**Mult**	**dE (cm-1)**	**5**	**3**	**1**
1–1	1	3	0	0.12	0.88	0
2–3	2	3	56.2	0.1	0.9	0
4–5	2	5	1270.9	1	0	0
6–7	2	5	1403	0.9	0.1	0
8–8	1	5	1439.5	0.88	0.12	0
9–10	2	5	7339.1	0.97	0.03	0
11–12	2	5	7392.2	0.98	0.02	0
13–13	1	5	7409.5	0.99	0.01	0
14–14	1	1	8370.4	0	0.06	0.94
15–15	1	1	9138.5	0	0.03	0.97
16–16	1	3	10235.5	0.02	0.97	0
17–17	1	3	10258.9	0.02	0.98	0
18–19	2	3	10328.6	0.01	0.99	0
20–20	1	3	10466.2	0.01	0.97	0.02
21–21	1	3	10499.4	0	0.96	0.04
22–22	1	3	12099.1	0.02	0.96	0.02
23–23	1	3	12126.9	0.02	0.98	0
24–25	2	3	12207.6	0.02	0.98	0
26–26	1	3	12334.9	0.02	0.98	0.01
27–27	1	3	12344.2	0.01	0.97	0.01
28–28	1	1	14089	0	0.03	0.97
29–30	2	5	14659.8	1	0	0
31–31	1	5	14816.5	0.98	0.02	0
32–32	1	5	14820.4	0.98	0.02	0
33–34	2	5	14934.8	0.98	0.02	0
35–35	1	5	15004.6	0.98	0.02	0
36–36	1	5	15027.9	0.98	0.02	0
37–38	2	5	15062.5	0.99	0.01	0
39–40	2	3	16462.9	0	0.94	0.06

41–41	1	3	16478.1	0	1	0
42–43	2	1	17213.4	0	0.28	0.72
44–44	1	3	17358.6	0	0.99	0.01
45–45	1	3	17406.9	0	1	0
46–47	2	3	17478.9	0	0.82	0.17
48–48	1	3	17491.3	0	1	0
49–49	1	3	17493.6	0	1	0
50–50	1	3	18584.1	0.01	0.99	0
51–52	2	3	18592.9	0	0.97	0.02
53–55	3	3	18891.3	0	0.99	0
56–57	2	3	19844	0	0.99	0.01
58–58	1	3	19871.9	0	1	0
59–60	2	1	20895.1	0	0.14	0.86
61–61	1	3	21390.3	0.01	0.99	0
62–63	2	3	21480.3	0	0.88	0.11
64–64	1	3	21595.3	0	0.99	0
65–66	2	3	21637.9	0	0.97	0.03
67–67	1	1	24553.8	0	0.43	0.57
68–69	2	3	24650.2	0.01	0.98	0.01
70–70	1	1	24745	0	0.02	0.98
71–71	1	3	24772.1	0	0.58	0.42
72–72	1	1	25269	0	0.01	0.99
73–74	2	3	25533.1	0	0.97	0.03
75–75	1	3	25554.8	0	0.99	0
76–76	1	5	25950	0.96	0.04	0
77–77	1	5	25953.3	0.96	0.03	0
78–79	2	5	26039.9	0.97	0.03	0
80–80	1	5	26070.9	0.97	0.03	0
81–82	2	1	26595.7	0	0.05	0.95
83–83	1	3	28933.9	0.03	0.62	0.35
84–84	1	3	29056.7	0.01	0.98	0
85–85	1	3	29062	0	0.99	0.01
86–87	2	3	29081.1	0.02	0.98	0

88–88	1	3	29111.1	0.03	0.95	0.02
89–90	2	3	29244.4	0	1	0
91–91	1	3	29259.3	0	1	0
92–92	1	3	29418.1	0	0.6	0.4
93–93	1	1	29757.8	0	0.18	0.82
94–94	1	3	29939.5	0	0.99	0.01

Table S10. L^1 / Br, computed transitions, ζ = 415.

				Spin Projections		
States	**Deg**	**Mult**	**dE (cm-1)**	**5**	**3**	**1**
1–1	1	3	0	0.49	0.51	0
2–3	2	3	73.9	0.5	0.5	0
4–5	2	5	490.1	1	0	0
6–7	2	5	888.6	0.5	0.5	0
8–8	1	5	941.9	0.51	0.49	0
9–10	2	5	7396.3	0.97	0.03	0
11–12	2	5	7446.7	0.99	0.01	0
13–13	1	5	7463.1	0.99	0.01	0
14–14	1	1	8525.8	0	0.08	0.92
15–15	1	1	9305.4	0	0.04	0.96
16–16	1	3	10228.4	0.02	0.98	0
17–17	1	3	10245.5	0.02	0.98	0
18–19	2	3	10275.1	0.01	0.99	0
20–20	1	3	10361.8	0.01	0.97	0.02
21–21	1	3	10446	0	0.93	0.07
22–22	1	3	11828.3	0.04	0.95	0.01
23–23	1	3	11860	0.04	0.96	0
24–25	2	3	11943.2	0.04	0.96	0
26–26	1	3	12085.8	0.03	0.96	0.01
27–27	1	3	12096	0.03	0.96	0.01
28–29	2	5	13461.6	1	0	0
30–30	1	5	13632.7	0.97	0.03	0

31–31	1	5	13639.4	0.96	0.04	0
32–33	2	5	13756	0.96	0.04	0
34–34	1	5	13820	0.97	0.03	0
35–35	1	5	13846.1	0.96	0.04	0
36–37	2	5	13866.9	0.99	0.01	0
38–38	1	1	14170	0	0.03	0.97
39–39	1	3	15572.3	0	1	0
40–41	2	3	15577	0	0.98	0.02
42–42	1	3	16694.1	0	0.99	0.01
43–43	1	3	16729.7	0	1	0
44–45	2	3	16745.9	0	0.89	0.11
46–46	1	3	16881.9	0	1	0
47–47	1	3	16888.8	0	1	0
48–49	2	1	17069.1	0	0.25	0.75
50–50	1	3	17725.8	0	0.99	0
51–52	2	3	17756.5	0	0.92	0.07
53–53	1	3	18021	0	0.99	0
54–55	2	3	18037.3	0	0.97	0.03
56–57	2	3	18935.4	0	0.99	0.01
58–58	1	3	18951.9	0	1	0
59–60	2	3	20497.1	0	0.67	0.33
61–61	1	3	20606.2	0.01	0.99	0
62–63	2	1	20903.7	0	0.35	0.65
64–64	1	3	21133.1	0	0.99	0.01
65–66	2	3	21171.8	0	0.96	0.03
67–67	1	1	23676.7	0	0.04	0.96
68–68	1	1	23848.2	0	0.02	0.97
69–70	2	3	24241.4	0.03	0.95	0.02
71–71	1	3	24285.2	0.04	0.93	0.03
72–72	1	1	24311.8	0	0.01	0.99
73–73	1	5	24748.4	0.96	0.04	0
74–74	1	5	24755.3	0.96	0.03	0.01
75–76	2	5	24854.2	0.94	0.06	0

77–77	1	5	24892.8	0.94	0.06	0
78–79	2	3	25293.9	0	0.86	0.14
80–80	1	3	25362.1	0	1	0
81–82	2	1	25804.8	0	0.17	0.83
83–83	1	3	27671.9	0	0.99	0.01
84–84	1	3	27688.7	0.01	0.99	0
85–86	2	3	27723	0.01	0.98	0
87–87	1	3	27734	0.03	0.91	0.06
88–88	1	3	27759.1	0.02	0.96	0.02
89–89	1	3	28273.1	0	0.57	0.42
90–90	1	3	28652.9	0	0.99	0
91–92	2	3	28668	0	1	0
93–93	1	3	28674.2	0.01	0.99	0

Calculated zero-field splitting parameters

Table S11. Calculated *D* parameters, $\zeta = 415\ cm^{-1}$.

	L^2 / MeCN	**L^1 / MeCN**	**L^1 / Cl**	**L^1 / Br**
D [cm^{-1}]	28.1	36.5	56.2	73.9

References

1. A. Decker, J. U. Rohde, L. Que Jr. and E. I. Solomon, *J. Am. Chem. Soc.*, 2004, **126**, 5378-5379.
2. F. Neese, *Comput. Mol. Sci.* , 2012, **2**, 73-78.
3. F. Neese, *Comput. Mol. Sci.*, 2018, **8**.
4. F. Neese, F. Wennmohs, U. Becker and C. Riplinger, *J. Chem. Phys.* , 2020, **152**, 224108.
5. R. Ahlrichs and F. Weigend, *Phys. Chem.*, 2005, **7**, 3297-3305.
6. S. Grimme, J. Antony, S. Ehrlich and H. Krieg, *J. Chem. Phys.*, 2010, **132**, 154104.
7. M. Garcia-Ratés and F. Neese, *J. Comput. Chem.*, 2020, **41**, 922–939.
8. G. Nunn, M. A. Bates, M. C. R. Cockett and P. H. Walton, *manuscript in preparation*.